Monthly Notices
of the
ROYAL ASTRONOMICAL SOCIETY

MNRAS **463,** 63–77 (2016) doi:10.1093/mnras/stw1944
Advance Access publication 2016 August 8

Resolving flows around black holes: the impact of gas angular momentum

Michael Curtis★ and Debora Sijacki

Institute of Astronomy and Kavli Institute for Cosmology, University of Cambridge, Madingley Road, Cambridge CB3 0HA, UK

Accepted 2016 August 2. Received 2016 August 2; in original form 2016 June 9

ABSTRACT

Cosmological simulations almost invariably estimate the accretion of gas on to supermassive black holes using a Bondi–Hoyle-like prescription. Doing so ignores the effects of the angular momentum of the gas, which may prevent or significantly delay accreting material falling directly on to the black hole. We outline a black hole accretion rate prescription using a modified Bondi–Hoyle formulation that takes into account the angular momentum of the surrounding gas. Meaningful implementation of this modified Bondi–Hoyle formulation is only possible when the inner vorticity distribution is well resolved, which we achieve through the use of a super-Lagrangian refinement technique around black holes within our simulations. We then investigate the effects on black hole growth by performing simulations of isolated as well as merging disc galaxies using the moving-mesh code AREPO. We find that the gas angular momentum barrier can play an important role in limiting the growth of black holes, leading also to a several Gyr delay between the starburst and the quasar phase in major merger remnants. We stress, however, that the magnitude of this effect is highly sensitive to the thermodynamical state of the accreting gas and to the nature of the black hole feedback present.

Key words: black hole physics – methods: numerical – cosmology: theory.

1 INTRODUCTION

Gas falling on to supermassive black holes that reside in the centres of majority galaxies may have a significant amount of angular momentum with respect to the central black hole. The accreting gas will settle into orbits that are aligned with a plane normal to the mean angular momentum of the infalling gas. Once the fluid has settled on to circular orbits accretion on to the central object will be inhibited by the centrifugal force and, as such, a disc-like structure will form, with the subsequent evolution of the system governed by, amongst others, the viscous processes that are present in the disc (Pringle 1981; Frank, King & Raine 2002). The viscosity of the fluid causes inner packets of fluid to move inwards and, in doing so, they transfer angular momentum to the outer parts of the disc. This process causes most of the mass to spiral into the central object, whilst transporting angular momentum outwards.

One key problem with the predictive power of accretion disc theory is understanding the nature and relative importance of the different sources of viscosity. If we assume that the source of the viscosity is molecular then we can estimate the ratio of the inertial to viscous forces, the Reynolds number, as

$$Re = \frac{u_\phi R}{\nu}, \tag{1}$$

where u_ϕ is the rotational velocity of the fluid, $\nu \sim c_s\lambda$ is the molecular viscosity of the fluid, c_s is the sound speed of the gas and λ is the mean free path length. Putting in typical values for accretion discs yields a Reynolds number $\sim 10^{15}$, which implies an accretion time-scale larger than a Hubble time. Clearly, to explain the accretion rates on to observed active galactic nuclei (AGN), we need to invoke different viscosity mechanisms. These are likely to include magnetic effects, especially at small spatial scales, such as the magnetic rotational instability, which occurs in sufficiently ionized flows for which u_ϕ decreases as a function of radius (Balbus & Hawley 1991). In such cases, the effect is to negatively torque inner fluid elements, causing them to fall on to closer orbits, and vice versa. This motion is unstable and leads to a magnetic viscosity. Another source of viscosity may be caused by the turbulent motion of the disc, where the random flow and eddies of the turbulence lead to a viscosity analogous to that driven by random flow on the molecular level. The nature of such turbulence and at what point in the flow it sets in remains, however, a key uncertainty.

As there are still fundamental gaps in our understanding of gas angular momentum transport, we are limited in our ability to successfully model black hole accretion discs. Hence, much modern theory follows Shakura & Sunyaev (1973) in parametrizing the viscosity as $\nu = \alpha c_s H$, where H is the disc scaleheight and $0 < \alpha \lesssim 1.0$ is a dimensionless free parameter that essentially represents our ignorance about the exact nature of the viscosity. Within this framework one can solve the steady disc equations for the geometrically thin disc regime. While widely used this approximation is by no means necessarily true – it will be violated, for example, if radiative

★ E-mail: mc636@ast.cam.ac.uk

cooling is not efficient, leading to a family of advection dominated accretion flow (Abramowicz et al. 1995; Narayan & Yi 1995) or adiabatic inflow–outflow solutions (Blandford & Begelman 1999).

Gas angular momentum transport on galaxy-wide scales is also rather uncertain, even though is it believed that the black hole's local gas reservoir may need to be replenished during the black hole lifetime. While galaxy mergers and cosmic filamentary inflows have been convincingly advocated (Hernquist 1989; Barnes & Hernquist 1991; Birnboim & Dekel 2003; Kereš et al. 2005) as mechanisms of very efficient gas transport inwards to $\sim$ kpc scales, the exact magnitude of these processes is affected by star formation efficiency, as well as by the nature of stellar and black hole feedback processes (e.g. Springel, Di Matteo & Hernquist 2005; van de Voort et al. 2011; Dubois et al. 2013; Nelson et al. 2015). On sub-kpc scales, an array of physical mechanisms have been invoked to explain the successive gas angular momentum transport. These include global and local bar and spiral instabilities (Roberts, Huntley & van Albada 1979), with the possibility of a 'bars-within-bars' mechanism (Shlosman, Frank & Begelman 1989), clumpy, turbulent discs (King & Pringle 2006; Krumholz, McKee & Klein 2006; Hobbs et al. 2011) or discs supported by radiation pressure (Thompson, Quataert & Murray 2005). While the feasibility of some of these mechanisms has been studied by means of high-resolution cosmological or isolated galaxy simulations (e.g. Mayer et al. 2007; Levine et al. 2008; Hopkins & Quataert 2010; Emsellem et al. 2015), gas angular momentum transfer within self-gravitating discs remains an unsolved issue (Goodman 2003).

It is thus unsurprising that currently, most cosmological simulations estimate the growth of black holes by use of a Bondi–Hoyle–Lyttleton approach (Hoyle & Lyttleton 1939; Bondi & Hoyle 1944; Bondi 1952), adopting the formula

$$\dot{M} = \frac{4\pi G^2 M_{\rm BH}^2 \rho_\infty}{\left(c_\infty^2 + v_\infty^2\right)^{3/2}}, \tag{2}$$

where $M_{\rm BH}$ is the mass of the black hole, c_∞ and ρ_∞ are the sound speed and gas density at infinity and v_∞ is the relative velocity between the black hole and the gas at infinity. Clearly, this does not take into account the effect of gas angular momentum. Doing so is difficult – in galaxy formation simulations we cannot directly resolve the relevant scales required to understand the accretion flows in regions close to the black hole (i.e. in the sub-kpc or sub-parsec regime) and, as discussed above, even if we could we are fundamentally limited by our understanding of the physical processes on these scales. What is required to improve on the Bondi–Hoyle–Lyttleton approach in cosmological simulations is a simple theoretical framework that links how the accretion rate on small scales may be affected by the mean angular momentum of the in-falling gas on large scales.

There have been several attempts to account for the effects of angular momentum on the black hole accretion rate within galaxy formation simulation. Power, Nayakshin & King (2011) use an accretion disc particle technique, whereby gas particles of sufficiently low angular momentum that their orbits would cross a specified accretion radius are added to a particle that accounts for the unresolved inner accretion disc. The black hole then accretes matter from this disc on some viscous time-scale. Rosas-Guevara et al. (2015) make similar assumptions, and calculate the net tangential velocity of accreting material and compare this to the sound speed of the gas. For sufficiently high gas angular momentum, the traditional Bondi rate is suppressed.

In this paper we adopt an alternative method, based on the work of Krumholz et al. (2005) (for previous related works see also Abramowicz & Zurek 1981; Proga & Begelman 2003), who parametrize the accretion rate on to a central object in terms of the vorticity of the gas on large scales. The effect of increased vorticity is to suppress the accretion rate from the standard Bondi rate, as gas with a larger impact parameter than the accretion radius of the black hole circularizes before it can cross the horizon and forms a disc. In the limit of no vorticity, the prescription reduces to the spherically symmetric Bondi accretion case.

We implement this vorticity-based accretion rate prescription in the moving mesh code AREPO. After validating our implementation on a number of stringent tests, we investigate how this affect the accretion rate on to supermassive black holes in simulations of isolated galaxies, as well as of some simple galaxy binary mergers. In doing so, we make use of the refinement technique as described by Curtis & Sijacki (2015), which allows us to improve the resolution of the fluid flow around black holes in our simulations. Accurately resolving the velocity structure of the gas in this region is vital for successfully implementing the vorticity prescription and we show how failing to do so leads to an underestimate of the vorticity. Whilst this work focuses on galaxy-scale simulations, we intend to present a method for use in fully cosmological simulations.

This paper is organized as follows. In Section 2, we outline our methodology and the exact nature of our new implementation. In Section 3, we discuss analytical expectations of the vorticity-based accretion rate prescription on the dynamical models of black hole growth. We then present several numerical experiments in Section 4 to validate our numerical implementation, before showing the main results of our work in Section 5 where both isolated and merging galaxy simulations are discussed. Finally, Section 6 presents our conclusions and plans for future work.

2 METHODOLOGY

2.1 Code

2.1.1 Basic setup

We use the moving-mesh code AREPO code (Springel 2010) for all simulations in this paper. AREPO employs the TREEPM approach (Springel et al. 2005) for handling gravitational interactions, and dark matter is represented by a collisionless fluid of massive particles. The fluid is modelled using a quasi-Lagrangian finite volume technique whereby the gas is discretized by tessellating the computational domain with a Voronoi mesh.

Star formation is carried out using the model of Springel & Hernquist (2003). We stochastically form star particles from cells of gas above a density threshold of $\rho_{\rm sfr} = 0.18\,{\rm cm}^{-3}$, with a characteristic time-scale of $t_{\rm sfr} = 1.5\,{\rm Gyr}$. Once formed, star particles only interact gravitationally with other particles. The unresolved thermal and turbulent processes that occur in the interstellar medium (ISM) are assumed to result in a self-regulated equilibrium described by an effective equation of state. We adopt two different such equations: the most commonly used multiphase model with a 'stiff' equation of state ($q_{\rm EOS} = 1$ in the notation of Springel & Hernquist 2003), as well as a softer equation of state with $q_{\rm EOS} = 0.1$, which interpolates between $q_{\rm EOS} = 1$ and an isothermal medium of temperature 10^4 K, and which corresponds to a less pressurized and more clumpy medium. In addition to this, in some simulations we include metal line cooling as in Vogelsberger et al. (2013), where we assume that the gas has a solar abundance, since we are primarily interested in the qualitative range of any subsequent effects. The variations of the ISM model we consider here are aimed at addressing the possible

impact of the gas thermodynamical state on the subsequent nature of the accretion flow and hence black hole growth.

2.1.2 *Black hole refinement scheme*

In order to improve the resolution of the simulation in the region of black hole particles, we employ the black hole refinement scheme of Curtis & Sijacki (2015). This makes use of the ability of AREPO to split and merge cells based on arbitrary criterion by forcing cells to decrease linearly in radius as they approach the black hole. This means that for cells a distance d from a black hole particle have a cell radius R, where

$$\frac{d}{R_{\rm ref}}\frac{\left(R^{\rm cell}_{\rm max}-R^{\rm cell}_{\rm min}\right)}{c}+\frac{R^{\rm cell}_{\rm min}}{c}<R, \tag{3}$$

$$\frac{d}{R_{\rm ref}}\left(R^{\rm cell}_{\rm max}-R^{\rm cell}_{\rm min}\right)+R^{\rm cell}_{\rm min}>R. \tag{4}$$

Here, $R_{\rm ref}$ is the scale over which refinement occurs, which we typically set to be equal to the black hole smoothing length, c is a constant that we set to 2, whilst $R^{\rm cell}_{\rm min}$ and $R^{\rm cell}_{\rm max}$ determine the aggression of the refinement. We typically set these to be equal to the Bondi radius and the black hole smoothing length, respectively.

2.2 Black hole model

We adopt the model of Curtis & Sijacki (2015), based upon Di Matteo, Springel & Hernquist (2005), Springel et al. (2005) to follow the evolution of black holes. We compare our vorticity-based prescription outlined below to that of the standard Bondi-like formula

$$\dot{M}_{\rm Bondi}=\frac{4\pi G^2M^2_{\rm BH}\rho_\infty}{c^3_\infty}, \tag{5}$$

where we do not take into account the relative velocity term in this work. Moreover in all simulations we limit the accretion on to the black hole to the Eddington limit

$$\dot{M}_{\rm Edd}\equiv\frac{4\pi GM_{\rm BH}m_{\rm p}}{\epsilon_{\rm r}\sigma_{\rm T}c}, \tag{6}$$

where σ_T is the Thomson cross-section, $m_{\rm p}$ is the mass of a proton and $\epsilon_{\rm r}=0.1$ is the radiative efficiency.

In this paper, feedback is injected by adopting several different mechanisms, as we are interested in the effect that this choice has on the magnitude of the black hole growth suppression given by our vorticity implementation. This is driven by the fact that we expect that, at high sound speeds, the suppression will be greatly reduced. We proceed by coupling a fraction $\epsilon_{\rm f}$ of the luminosity to the gas, leading to an energy budget of

$$\Delta E_{\rm feed}=\epsilon_{\rm f}\epsilon_{\rm r}\Delta M_{\rm BH}c^2. \tag{7}$$

Here, $\epsilon_{\rm f}=0.05$ is the feedback efficiency, which is set to reproduce the normalization of the locally inferred $M_{\rm BH}$–σ relation (Di Matteo et al. 2005; Sijacki et al. 2007).

We allow for feedback to occur both isotropically (pure thermal coupling) and in a bipolar manner. In the latter case, we inject mass, energy and momentum within a cone of opening angle $\theta_{\rm out}=\pi/4$ which is aligned with the net angular momentum axis of the accreting gas. In this case, the black hole is restricted to accrete from the cold disc and we estimate the accretion rate using parameters derived from this component. In bipolar simulations when a cold disc is very sub-dominant, we proceed as in the isotropic case. For full details, see Curtis & Sijacki (2015).

2.2.1 *Vorticity implementation*

The benefits of the refinement method mean that in principle it is possible to account for the angular momentum of the gas in different ways (Power et al. 2011; Rosas-Guevara et al. 2015). In this paper we implement the unified model of Krumholz et al. (2005), which is very well suited to our computational approach. For completeness, we briefly summarize the method here. The authors consider an accreting point particle of mass M within a velocity field of finite vorticity at infinity, which they parametrize as

$$\boldsymbol{v}_\infty=\omega_\star c_\infty\frac{y}{r_{\rm B}}\,\hat{\boldsymbol{x}}\,, \tag{8}$$

where $r_{\rm B}$ is the Bondi radius, c_∞ is the sound speed of the gas at infinity, and $\omega_\star$ is a dimensionless 'vorticity parameter', so called because the vorticity of the flow is $-\omega_\star c_\infty/r_{\rm B}\,\hat{\boldsymbol{z}}$, where we have assumed a Cartesian coordinate system centred on the black hole. The task is then to analyse the accretion as a function of $\omega_\star$. For $\omega_\star=1$, gas with impact parameter equal to the Bondi radius is travelling at the Keplerian velocity. This suggests that there is a transition region around $\omega_\star=1$, which leads Krumholz et al. (2005) to consider three regimes of accretion.

(i) Very small $\omega_\star$, where original Bondi accretion holds.
(ii) Small $\omega_\star$.
(iii) Large $\omega_\star$.

2.2.1.1 Very Small $\omega_\star$. As the work attempts to build on the Bondi formula, it is useful to consider first the cut-off for which the angular momentum is too small to have an effect. Krumholz et al. (2005) argue that if the gas only circularizes at a radius that is less than that of the accreting object (in this case the Schwarzschild radius, $r_{\rm s}$, as we consider non-spinning black holes) then the material will be accreted on mostly radial orbits. This implies a condition for when the original Bondi rate is appropriate

$$r_{\rm circ}=\omega^2_\star y^4/r^3_{\rm B}<r_{\rm s}, \tag{9}$$

which implies

$$\omega_\star<\omega_{\rm crit}\equiv\sqrt{r_{\rm s}/r_{\rm B}}, \tag{10}$$

as the condition for the original Bondi prescription to hold.

2.2.1.2 Small $\omega_\star\ll1$, $\omega_\star>\omega_{\rm crit}$. Above the critical vorticity derived in the previous section, the gas will circularize before it reaches the accretor. In these cases, the analysis of Krumholz et al. (2005) suggests that the resulting torus that forms will extend to $r_{\rm B}$ with a scaleheight of $\sim r_{\rm B}$, thus blocking accretion in the range $\pi/4<\theta<3\pi/4$, i.e. in the plane of the gaseous disc. This has the effect of decreasing the accretion rate to $\dot{M}\sim0.3\dot{M}_{\rm Bondi}$.

2.2.1.3 Large $\omega_\star\geq1$. For the final case, that of a high vorticity, Krumholz et al. (2005) argue that accreted material will lie on streamlines that bend sharply, shocking the gas and allowing it to lose energy and fall on to the central particle. This will occur on streamlines that have a larger peak escape velocity than the velocity of the gas at infinity. The accretion rate can then be deduced by summing the gas entering an area A where the condition is satisfied, that is

$$\dot{M}\approx\int_A\rho_\infty\sqrt{v_\infty(y,z)^2+c^2_\infty}\,{\rm d}y\,{\rm d}z, \tag{11}$$

which, when calculated, gives

$$\dot{M}(\omega_\star) \approx 4\pi r_{\rm B}^2 \rho_\infty c_\infty f(\omega_\star), \tag{12}$$

where $f(\omega_\star)$ is a numerical factor that is approximated in the limit $\omega_\star \to \infty$ by

$$f(\omega_\star) \approx \frac{2}{3\pi\omega_\star}\ln(16\,\omega_\star). \tag{13}$$

We implement this scheme into the AREPO code. We calculate the vorticity parameter as

$$\omega_\star = |\boldsymbol{\omega}|\frac{r_{\rm B}}{c_\infty}, \tag{14}$$

by taking an exponential spline kernel-weighted (Monaghan & Lattanzio 1985) mean of the vorticities of the neighbouring cells to the black hole.[1] We then calculate the accretion rate whenever $\omega_\star > \omega_{\rm crit}$ using the following expression

$$\dot{M}_{\rm Vort} = \frac{4\pi G^2 M_{\rm BH}^2 \rho_\infty}{c_\infty^3} \times \begin{cases} 0.34 & \omega_\star < 0.1 \\ 0.34\frac{2}{3\pi\omega_\star}\ln(16\omega_\star) & \omega_\star > 0.1. \end{cases} \tag{15}$$

since the analytic expression is well fit by a piecewise approximation for $\omega_\star$ greater and less than 0.1. The factor of 0.34 accounts for the same phenomenon detailed in Section 2.2.1.2, selected to match the value of $0.3\dot{M}_{\rm Bondi}$ for $\omega_{\rm crit} < \omega_\star \ll 1$. It differs from exactly 0.3 because of a slight difference between equation (12) and the standard Bondi rate.

2.3 Initial conditions

In order to understand the implications of our implementation, we have carried out a series of simulations of an isolated disc galaxy. This simulation setup is particularly well suited to our topic of inquiry as, on large scales, the majority of gas will be rotationally supported and thus the effect of gas angular momentum on the black hole accretion rate may be significant. In fact, the observed luminosities of local AGN harboured within spiral galaxies are either rather low or modest, and in the latter case often fall within the category of Seyferts, suggesting limited fuelling rates possibly driven by bar instabilities (see e.g. Knapen, Shlosman & Peletier 2000; Laine et al. 2002; Kewley et al. 2006).

Our initial conditions match those of Curtis & Sijacki (2015, for original implementation of the model and further details see Springel et al. 2005). These consist of an isolated galactic disc in hydrostatic equilibrium, situated within a dark matter halo described by a Hernquist (1990) density profile

$$\rho_{\rm dm} = \frac{M_{\rm dm} a}{2\pi r(r+a)^3}, \tag{16}$$

where $M_{\rm dm}$ is the total dark matter mass and a is a scaling parameter. We generate a self-consistent gaseous disc distribution in equilibrium and potential by an iterative process, based on an exponential surface density profile, with the azimuthal velocity set to

$$v_{\phi,{\rm gas}}^2 = R\left(\frac{\partial\Phi}{\partial R} + \frac{1}{\rho_{\rm gas}}\frac{\partial P}{\partial R}\right), \tag{17}$$

and the remaining velocity components $v_R = v_z = 0$. We also include a centrifugally supported stellar disc that also follows an exponential surface density profile. Our parameters are chosen to represent a simplified Milky Way-like galaxy, but note that we do not attempt to explicitly model Sagittarius A* in any way.

In the last part of this paper we contrast our isolated disc simulations with simulations of binary galaxy mergers. We consider only equal mass mergers on prograde parabolic orbits and initial galaxy properties that are identical to our isolated galaxy setup. These simulations serve to explore the difference in black hole growth reduction due to the vorticity-based accretion rate prescription in the case where large-scale gravitational torques affect the central gas density and angular momentum distribution significantly.

In Table 1 we list all simulations of isolated and merging galaxies used in this work, where we summarize the initial number of gas cells, type of refinement method, black hole accretion and feedback prescriptions and any other variations in the models, which relate to black hole seed mass, type of radiative cooling and the effective equation of state for the ISM.

3 ANALYTIC RESULTS: EXPECTED SUPPRESSION OF BLACK HOLE GROWTH

The black hole accretion rate, for both the vorticity and the standard Bondi rate prescription, is highly sensitive to the gas sound speed, gas density and the black hole mass. Probing the full parameter space with numerical simulations is non-viable, both because of the non-linear nature of the evolution but also because of the significant computational time to carry out an individual simulation. To tackle this, we here explore the effects of changing the gas and black hole properties in the context of our isolated galaxy setup (see Section 2.3) and we subsequently explore part of the parameter space with fully self-consistent simulations.

It should be noted here that in both observations and simulations the exact nature of the gas close to the black hole's Bondi radius is poorly understood (Frank et al. 2002; Goodman 2003). While a number of recent studies constrain gas properties close to the Bondi radius in some systems, such as Sagittarius A* (Yuan, Quataert & Narayan 2003; Xu et al. 2006), M87 (Russell et al. 2015) or typically in LINERs and Seyferts through mega-masers (for a review see Lo 2005), we do not yet have a consensus on the density, temperature and velocity distribution of the gas. Thus for the following analysis, we make a very simplifying assumption and consider that the gas velocity field matches the initial (numerically derived) conditions down to the Bondi radius (see equation 17), although we also investigate the effect of assuming a field with a higher vorticity. The vorticity profile scales approximately as $\boldsymbol{\omega} \sim (R^{0.5})\hat{\boldsymbol{z}}$ with radius.

3.1 Expected suppression factor

In Fig. 1, coloured 2D histograms show the ratio of the vorticity-suppressed black hole accretion rate to the standard Bondi rate as a function of gas density and sound speed, for two fixed black hole masses of $3.8 \times 10^5\,{\rm M}_\odot$ (our default seed mass) and $10^7\,{\rm M}_\odot$, in the left-hand and right-hand panels, respectively. Here, we have included the effect of limiting the black hole growth by capping the accretion rate at the Eddington limit, hence the suppression

[1] Note that we have explored different choices of how many neighbouring gas cells to consider (e.g. within 0.1, 0.3, 0.5 and 1 of the black hole's smoothing length). While the exact value of the vorticity estimate may in some cases be sensitive to this choice, we found that our estimate of the accretion rate for all our results using super-Lagrangian refinement were robust and largely unchanged. This is further supported by our analytic estimates presented in Section 3.

Table 1. Simulation details for isolated and merger galaxy models, as indicated in the first column. The second column lists the initial number of gas cells employed (note that due to super-Lagrangian refinement this number can increase significantly during the simulated time-span). The third column indicates for which models we use our super-Lagrangian refinement around black holes (Yes) and for which we only use the standard (de)/-refinement present in AREPO (NO). The fourth and fifth columns indicate our adopted model for black hole accretion and feedback, while in the sixth column we list any other variations considered, such as the metal line cooling in addition to the primordial cooling (which is always switched-on), a softer equation of state (sEOS) for the ISM and a larger black hole seed mass of $10^7\,\mathrm{M}_\odot$, instead of our default choice of $3.8\times10^5\,\mathrm{M}_\odot$.

Type	$N_{\rm gas}$	Refinement	Accretion	Feedback	Additions
Isolated	10^5	No	Bondi	No	–
Isolated	10^5	Yes	Bondi	No	–
Isolated	10^5	No	Bondi	Thermal	–
Isolated	10^6	No	Bondi	Thermal	–
Isolated	10^7	No	Bondi	Thermal	–
Isolated	10^5	Yes	Bondi	Thermal	–
Isolated	10^6	Yes	Bondi	Thermal	–
Isolated	10^7	Yes	Bondi	Thermal	–
Isolated	10^5	Yes	Bondi	No	Metal line cooling
Isolated	10^5	Yes	Vorticity	No	Metal line cooling
Isolated	10^5	Yes	Bondi	No	sEOS
Isolated	10^5	Yes	Vorticity	No	sEOS
Isolated	10^5	Yes	Bondi	No	$M_0 = 10^7\,\mathrm{M}_\odot$
Isolated	10^5	Yes	Vorticity	No	$M_0 = 10^7\,\mathrm{M}_\odot$
Isolated	10^5	No	Vorticity	Thermal	–
Isolated	10^5	Yes	Vorticity	Thermal	–
Isolated	10^5	Yes	Bondi	Bipolar	sEOS
Isolated	10^5	Yes	Vorticity	Bipolar	sEOS
Merger	10^5	Yes	Bondi	No	Metal line cooling
Merger	10^5	Yes	Vorticity	No	Metal line cooling
Merger	10^6	Yes	Bondi	No	Metal line cooling
Merger	10^6	Yes	Vorticity	No	Metal line cooling

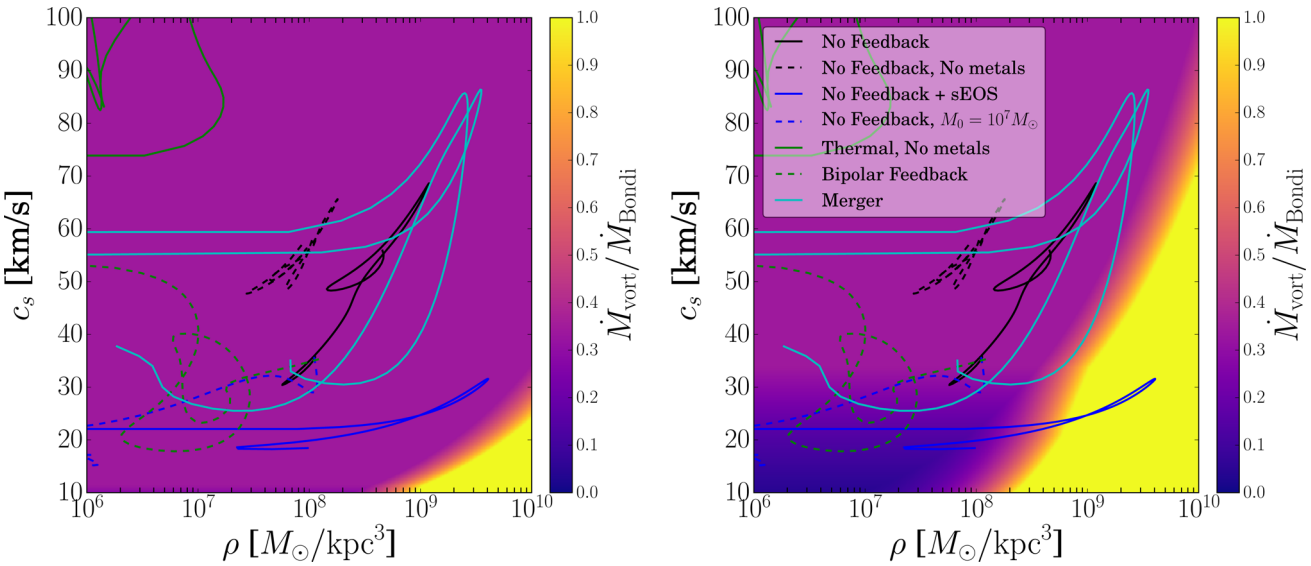

Figure 1. Coloured 2D histograms showing the ratio $\min(\dot{M}_{\rm Vort}, \dot{M}_{\rm Edd})/\min(\dot{M}_{\rm Bondi}, \dot{M}_{\rm Edd})$ for two fixed black hole masses of $3.8\times10^5\,\mathrm{M}_\odot$ (left-hand panel) and $10^7\,\mathrm{M}_\odot$ (right-hand panel) as a function of gas density and sound speed (see equation 15), assuming a given gas vorticity profile. Overplotted, we show the tracks from several of our simulation models, indicating the typical regimes simulated black holes are in (but note that simulated black hole masses grow with time along the shown tracks). In the bottom-left region of the parameter space, for high densities and low sound speeds (coloured yellow), the Eddington rate is the dominant limitation of the accretion rate, as the Bondi rate is very high. However, unless the sound speed is sufficiently small to allow for a large value of $\omega_\star$, the suppressing effect of the vorticity is limited to 0.34. As such, the resulting suppression is sensitive to the presence and type of feedback injected, as well as the ISM physics. There is also a dependence on the mass of the central black hole, as this affects the Bondi radius. Higher mass black holes present larger regions of the parameter space with high suppression, but also a larger region in which the black hole growth is Eddington limited.

is $\min(\dot{M}_{\rm Vort}, \dot{M}_{\rm Edd})/\min(\dot{M}_{\rm Bondi}, \dot{M}_{\rm Edd})$. This means that for sufficiently low sound speeds and high densities, the effective suppression is zero because the growth is Eddington limited, rather than being constrained by the angular momentum barrier (see yellow regions on the panels). At the other end of the spectrum, we note that for the majority of the parameter space the suppression ratio is at most 0.34. This is because, even for large black hole masses, the condition that the effective impact parameter be less than the accretion radius of the black hole (see Section 2.2.1.1) is not satisfied given our assumption on the velocity field of the gas. Indeed, we shall see later that this condition is particularly difficult to satisfy, even when large-scale torques during a major merger drive a substantial mass of gas to the central region of the galaxy. For the black hole with a higher mass there is a small region of the parameter space for which the suppression is especially high (see dark blue region on the right-hand panel) – this is driven by the increase in the Bondi radius of the black hole. Increasing the vorticity over that of our model by a factor of 10 has a similar effect, increasing the expected suppression for sound speeds less than 20 km s^{-1} and slightly shrinking the region which is Eddington limited.

On both plots, for context, we also show a selection of tracks from our simulations, to indicate the typical properties of the gas surrounding the black hole. Note however that in simulations black hole mass is not constant and thus to provide some guidance on the magnitude of the effect we over plot the same tracks on both panels. The assumptions we make about black hole feedback, as well as the cooling physics of the surrounding gas and the ISM clumpiness, can have significant consequences for the suppression we expect. The simulations with no feedback show a tight relationship between sound speed and density. This is not surprising, as we assume that gas that is sufficiently dense to be star-forming follows an effective equation of state Springel & Hernquist (2003), which has the effect of forcing the gas to higher sound speeds at larger densities. We can vary this by using a softer equation of state for the ISM – the track for this simulation (dark blue, solid) reaches much lower sound speeds.

On the other hand, thermal feedback distributed isotropically (green, solid) has the effect of dramatically heating the surrounding gas – especially that which is closest to the black hole. Whilst this itself has the effect of reducing the accretion rate, it means that such simulations are never in the regime that allows for strong angular momentum-driven suppression according to our model. If we restrict the feedback to a bipolar cone (green, dashed) – explicitly decoupling the heated gas from a cold, accreting gas disc, we can reach regimes where suppression is significant.

This strong dependence on the temperature of the gas is unsurprising when we note that the amount that we suppress the standard Bondi rate is proportional to $\omega_\star$, where:

$$\omega_\star \propto \frac{|\boldsymbol{\omega}|}{c_{\rm s}^3}. \tag{18}$$

Whilst some of the viscous processes that transport angular momentum might be expected to increase with increased thermal motions of the gas, we are fundamentally limited by of our treatment of the ISM. Improving our modelling of the gas physics to self consistently resolve a realistic multiphase ISM is the subject of much ongoing research – in the future it will certainly be interesting to see how this will affect our understanding of the gas properties around the black hole.

3.2 Expected delay in black hole growth

Because of the non-linear nature of black hole growth within simulations, looking at the ratio of the vorticity-based accretion rate to the standard Bondi rate alone can be a misleading guide to the results of simulations. This is principally because of two effects. First, the Bondi rate itself can vary dramatically with density and (in particular) sound speed of the ambient medium. As such, if the black hole is growing either very fast or very slow, then the final black hole mass will be dominated by the changes in the Bondi rate itself, and the black hole growing according to the vorticity prescription will undergo similar growth with a slight delay. Secondly, any early growth in black holes is compounded at later times, because of the M^2 dependence of the Bondi rate. This is a problem that will be particularly acute in simulations without strong self-regulation, which is the case for a variety of different models of feedback and, of course, for simulations without strong black hole feedback at all.

For this reason, we have carried out a series of simplified time integrations of black hole growth. We make several basic assumptions: in particular we do not include the effects of black hole feedback and we assume that the distribution of gas properties as a function of radius remains the same over time. We start the black holes at an initial seed mass and at each time step we calculate the updated accretion rate based on sampling the relevant gas properties at the Bondi radius (which grows with time), and continue the integrations for a maximum of 14 Gyr. We will see that whilst the results from simulated galaxies differ from these predictions in certain key ways, we are able to reproduce the general effects of using the vorticity prescription over a wide range of parameters.

In the left-hand panel of Fig. 2, 2D coloured histogram shows the delay in Gyr for a 3.8×10^5 $M_\odot$ black hole to increase its mass by an order of magnitude, as a function of gas density and sound speed (and keeping our default choice of gas vorticity distribution). The distribution is clearly peaked, with a well-defined maximum delay region, which we have overplotted for different values of the initial black hole mass. The parameter space for each is split into separate regions: in the top left (white region), for high sound speeds and low densities, the black hole is unable to grow by any significant fraction. The opposite occurs for high densities and low sound speeds (blue region) – the black hole grows fast regardless of suppression. There is, however, a tight regime in which the delay in black hole growth can be particularly significant (yellow–pink region) and comparable to the Hubble time.

On the right-hand panel of Fig. 2, we show an analogous plot but for an increased gas vorticity, which is now 10 times higher at all radii. For a large region of parameter space, the resulting delay in black hole growth remains similar or slightly larger. The region in which we expect the most significant suppression increases in size, as the magnitude of the suppressing effect increases, but the region of the parameter space in which we expect significant delay is still relatively small. Finally, we note that for larger initial black hole masses lower gas densities and higher sound speeds lead to a similar effective delay.

4 SIMULATION RESULTS: VALIDATION OF IMPLEMENTATION

Whilst all simulations that attempt to implement sub-grid prescriptions face difficulty in resolving the gas properties around the black hole, accurately resolving a higher order quantity such as the velocity field is especially difficult. In this section we detail our numerical experiments to validate our implementation of the vorticity

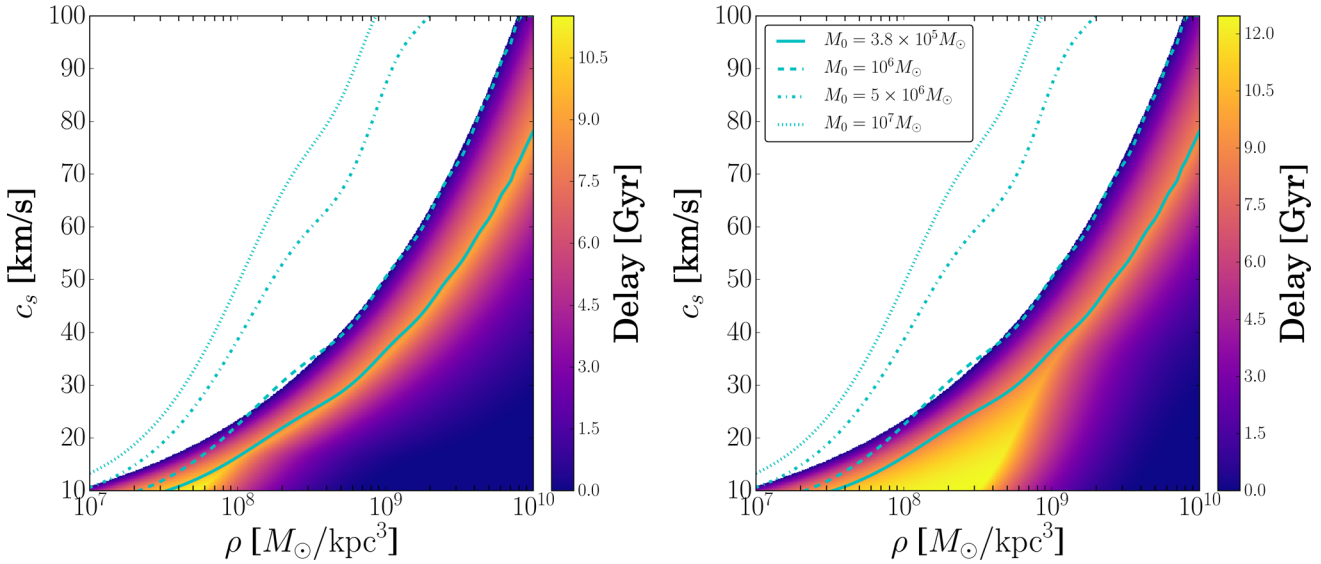

Figure 2. 2D coloured histograms showing the effective delay in Gyr for a 3.8×10^5 M$_\odot$ black hole to increase in mass by an order of magnitude for our default gas vorticity profile (left-hand panel) and assuming a vorticity that is an order of magnitude larger than our initial conditions (right-hand panel). We plot the peak of this distribution for a series of different starting black hole masses with lines of different styles, as indicated on the legend. At high sound speeds, and low densities, the black hole growth is insignificant. Conversely, for large densities and low sound speeds, the Bondi rate is sufficiently high that the black holes grow very fast, regardless of the suppressing effect of the vorticity prescription. In between there is a clearly defined region of the parameter space (yellow to pink shades) where the suppressing effect has a significant impact, causing delays in black hole growth comparable with the Hubble time. For higher starting black hole masses lower densities and higher sound speeds lead to similar delays. In practice, whether this occurs in simulations depends on the evolution of the surrounding gas, which is highly dependent on both the feedback routine and the ISM model chosen.

prescription within AREPO, whilst indicating limitations with the current approach. Whilst much of our discussion here is specific to the Krumholz et al. (2005) model, we note that our investigations raise points that are important for alternative approaches of angular momentum estimation in black hole accretion modelling.

4.1 Keplerian disc

In order to test the conservation properties of our refinement scheme, we simulate a cold, pressure free Keplerian disc. This problem, which holds modern hydrodynamics codes to a particularly stringent standard, is one that has been used to demonstrate the effects of systematic errors in angular momentum conservation (Cullen & Dehnen 2010; Hopkins 2015; Pakmor et al. 2016). In its latest version, which in particular adopts improvements to the gradient estimation and time integration, our moving mesh code AREPO shows very good conservation properties – for full details see Pakmor et al. (2016). Here, we are interested in the effects that our super-Lagrangian refinement scheme has on the gas angular momentum within the refinement region.

We adopt the same initial setup as Pakmor et al. (2016). In particular, we initialize a disc spanning a radial range of $0.5 < r < 2.0$ with gas density $\rho = 1.0$, and gas velocities $v_x = -yr^{-3/2}$, $v_y = xr^{-3/2}$. Here, the units used are arbitrary. Outside of this region, we set $\rho = 10^{-5}$ and $v = 0$. In both regions we set the internal energy to $u = 2.5^{-5}\gamma/\rho$, where we set the adiabatic index $\gamma = 5/3$. Our simulation uses a constant external gravitational acceleration of

$$g = -\frac{r}{r(r^2 + \epsilon^2)}, \tag{19}$$

where $\epsilon = 0.25$ for $r < 0.25$ and is zero otherwise. Since in this case there is no black hole particle, in the simulation with super-Lagrangian refinement we set the refinement region to be $R_{\rm ref} = 1.0$ and the maximum cell radius $R^{\rm cell}_{\rm max} = 10^{-2}$, which represents the size required for a smooth transition at the refinement boundary. We have tested different values for $R^{\rm cell}_{\rm min}$ – since the disc in this case does not extend to the centre of the simulation we find that our results are relatively insensitive to the exact value. For the plots here we show our simulation for which $R^{\rm cell}_{\rm min} = 10^{-4}$.

Fig. 3 illustrates the results for simulations both with (right-hand panel) and without (left-hand panel) our super-Lagrangian refinement scheme. We show the density across the disc at $t = 150$, and note the good agreement between the two simulations, which both show that the disc has remained stable for the entire duration of the simulation. In particular, the simulation with refinement shows somewhat more stable inner edge of the cold disc. The ratio of the total angular momentum of the disc to the initial theoretical value is plotted in the bottom row. Both simulations show very good conservation properties throughout, indicating that the cell refinement and de-refinement have not introduced neither significant angular momentum transport nor conservation issues. This is reassuring as it demonstrates that the estimation of gas angular momentum, and hence vorticity, does not suffer from spurious numerical artefacts due to our super-Lagrangian refinement.

4.2 Detecting spurious vorticity

The Krumholz et al. (2005) model assumes a large-scale disc-like vorticity and, thus for robustness of our scheme, we need to ensure not to take into account random turbulent vorticity that may be present in the simulations. This is especially problematic for radial flows (i.e. flows with negligible vorticity) close to the centre of the simulation domain, since the discrete nature of the velocity gradient calculation means that the small errors this introduces are amplified. As this is a function of both the limited resolution of the simulations, as well as the (Cartesian) coordinate system, we note here that this problem would not be avoided by using angular

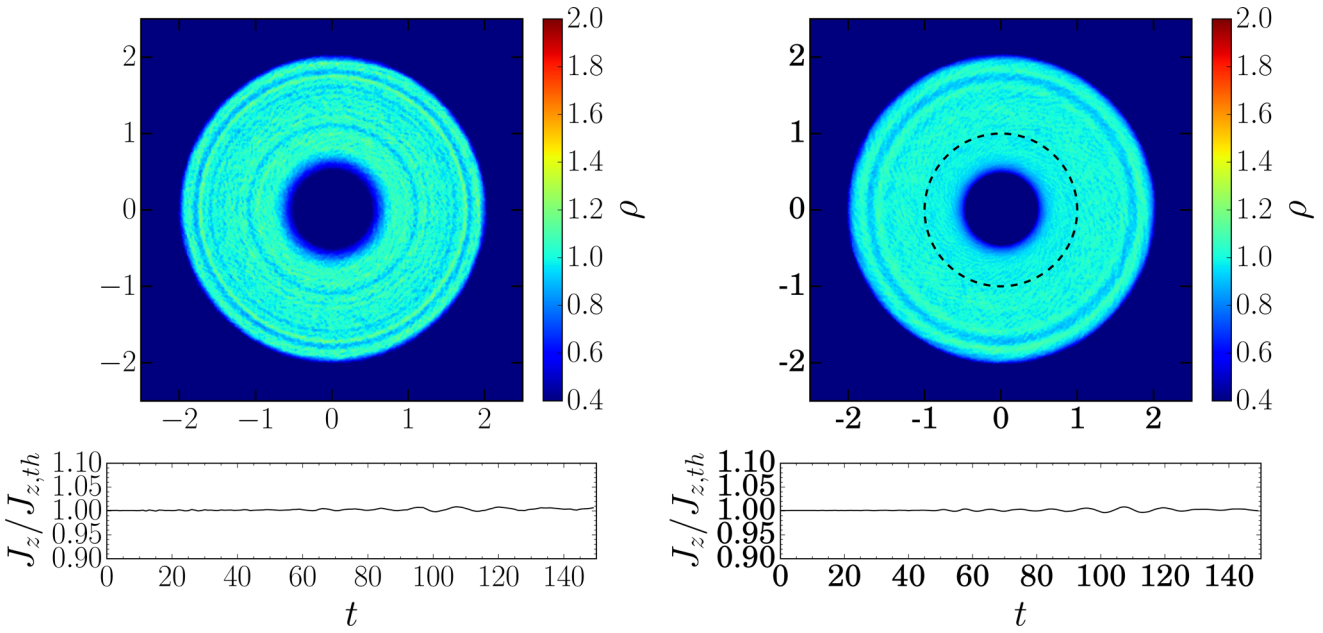

Figure 3. In the left-hand panel, we show the density map at $t = 150$ of a 2D simulation of a cold Keplerian disc for a simulation with no cell refinement or de-refinement (note that the units used are arbitrary). In the right-hand panel, we show an analogous plot, but for a simulation using our black hole refinement scheme, and the region within which we impose super-Lagrangian refinement is marked with a dashed circle. In both cases, we also show the ratio of the total angular momentum in the simulation to the initial theoretical value (bottom row). The simulations show very good conservation properties for the entire simulated time-span. In particular, the aggressive cell refinement and de-refinement do not cause any significant differences to the angular momentum conservation of the code.

momentum (or proxies for this, such as circular velocity of the gas) instead of vorticity – presence of minor anisotropies in the radial flow means that, in the central region, it is inevitable that gas with very large velocities on small but finite impact parameters will be present. In practice, in our simulations with more realistic initial conditions (such as of galaxies in isolated or cosmological settings), we find that this should rarely be an issue. Nevertheless, to avoid any spurious growth suppression, we ensure that the mean vorticity that we measure for the fluid is representative of a sufficiently large fraction of the gas mass. To do this, we compare the net vorticity within black hole's smoothing length with that of individual cells within the same region and calculate the fraction of the mass $f_{\rm sort}$ of the gas that has a vorticity within $\pi/4$ of the net direction. For a random distribution of vorticities, the mean value of $f_{\rm sort} \sim 0.15$. By examining the test simulations, we find that $f_{\rm sort} = 0.35$ represents a conservative threshold which minimizes the vorticity effects that are likely to be driven purely by noise. As such, for simulations with lower values of $f_{\rm sort}$ we use the standard Bondi accretion rate and not our vorticity prescription (for more details, see Appendix A).

Fig. 4 shows this phenomenon in practice. We show the velocity (first row) and vorticity (second row) fields for two simulations, one of a purely radial Bondi flow (left-hand column) and one with a coherent disc structure (right-hand column). We have scaled each simulation to the region of interest – that is, to a region that is comparable to the size of the black hole smoothing length. In each case, for context, we show a density slice across the $z = 0$ plane. For the Bondi simulation, the vorticity is essentially completely random, this being just the effect of the noise inherent in floating point arithmetic. The length of the arrows indicating the vorticity field have been normalized to the same value: in general, the size of these is amplified by the speed of the gas, which means that they are negligible except as the gas approaches the origin, where they blow up in size. Here, because of the steep velocity gradient, these errors are rapidly magnified, resulting in a spurious signal that we need to avoid. In the case of the isolated galaxy, we can see the rotating disc demonstrates a clear vorticity signal, aligned with the z-axis.

Our simple prescription based on $f_{\rm sort}$ works very well in detecting spurious vorticity and recovering the correct black hole growth rate, as shown in bottom row of Fig. 4. On the left, we plot both the ratio of instantaneous simulated black hole accretion rate to the analytical Bondi rate (top) as well as the ratio of the cumulative simulated to the cumulative analytical Bondi rate (bottom). Both of these ratios should be 1. Vorticity estimation without our $f_{\rm sort}$ prescription can lead to a significant accretion rate suppression, by more than an order of magnitude, which is purely driven by the numerical noise. Conversely, with our $f_{\rm sort}$ prescription, whilst there are occasions when (by chance) the vorticity alignment causes the rate to dip for a single time step, this basically makes no difference to the overall growth, as demonstrated by the bottom plot. In the right-hand bottom panel of Fig. 4, we show the mass fraction of gas which is aligned to the net vorticity direction as a function of time for isolated disc galaxy simulation with (dashed) and without black hole thermal feedback (the results are very similar in the case of the bipolar feedback). This confirms that spurious vorticity estimate is not an issue in these simulations, as for the vast majority of simulated time the mass fraction of gas aligned is much higher than $f_{\rm sort} = 0.35$.

4.3 Gas vorticity measurement in isolated disc galaxy models

All simulations that seek to account for the angular momentum of the gas in the black hole accretion rate must be able to robustly estimate the velocity field in the region of interest. Thus to demonstrate the validity of our approach, Fig. 5 shows radial profiles of the three velocity components (left-hand panel) and the corresponding radial vorticity profiles (right-hand panel) in

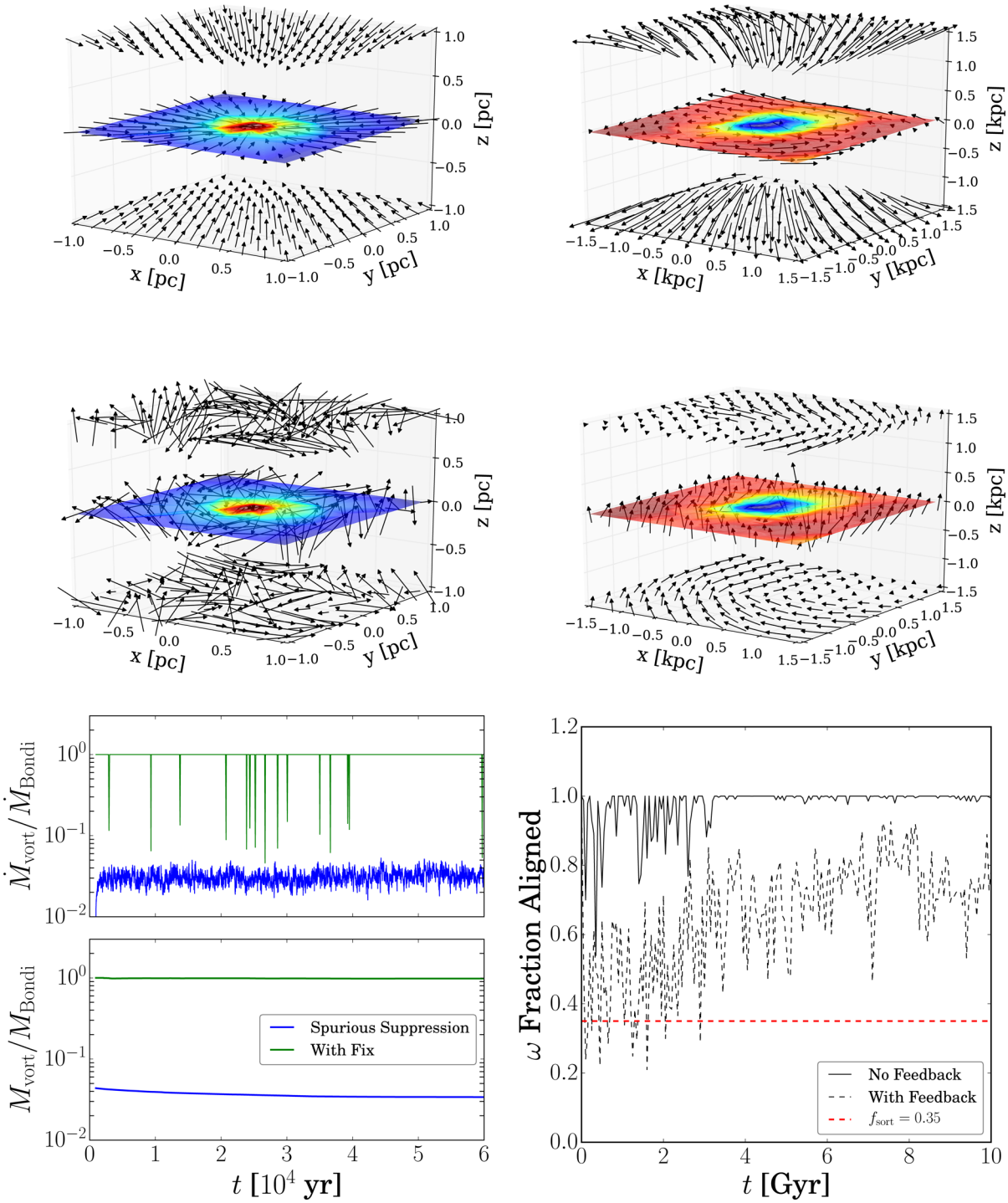

Figure 4. The top row shows the velocity field for simulations of an idealized Bondi inflow (left-hand column) and of an isolated disc galaxy with black hole feedback (right-hand column). In the second row, we show the corresponding vorticity field for the same simulations. In the case of the Bondi simulation, the arrows are normalized to a constant value. For context, we show a density slice in the $z = 0$ plane. In the Bondi case, the velocity field is entirely radial, but because of the discontinuity of the gradients in the centre of the simulation domain coupled with the rising velocity magnitude, the simulation results are increasingly sensitive to small errors in the gradient calculation. The resulting vorticity field is entirely noise driven, but can lead to a significant spurious signal. In the case of the isolated galaxy, the velocity structure of a disc is clearly defined, leading to a coherent, robust corresponding signal in the vorticity (aligned with the z-axis). In the bottom left-hand panels, we show both the instantaneous and cumulative accretion rate normalized to the analytical Bondi rate with and without our $f_{\rm sort}$ prescription used to minimize the noisy vorticity estimate. In the Bondi simulation our $f_{\rm sort}$ prescription is needed and recovers the correct accretion rate. In the isolated disc galaxy simulation, both with and without black hole feedback, spurious vorticity is rarely significant as shown in the bottom right-hand panel, where the mass fraction of gas aligned with the net vorticity direction as a function of time is plotted.

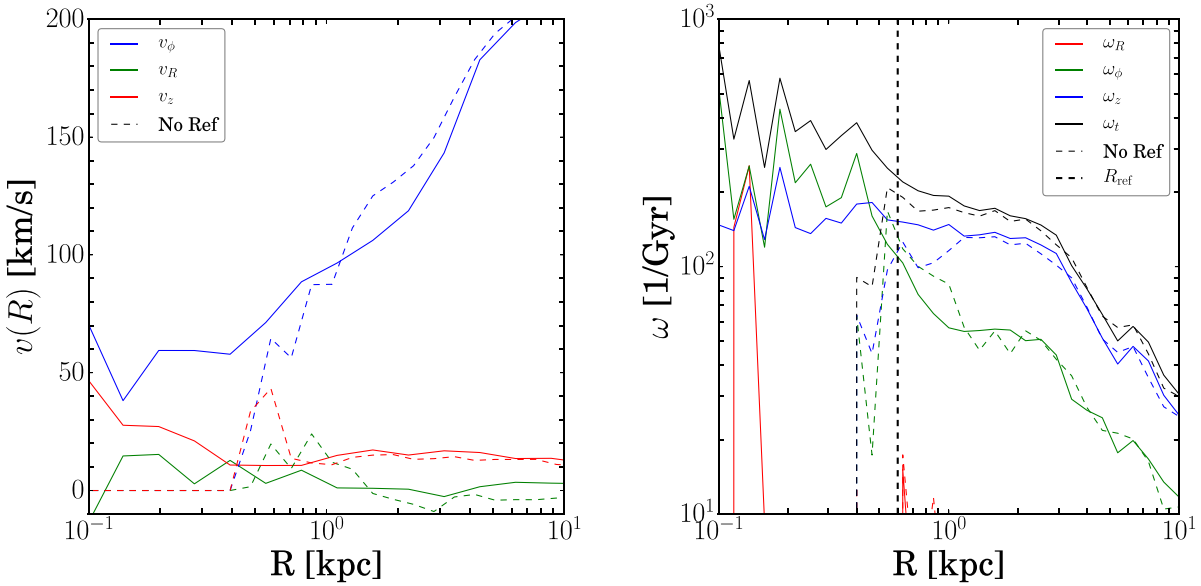

Figure 5. The left-hand panel shows radial profiles of the three velocity components in cylindrical (note that v_z represents the absolute velocity value) polar coordinates from a simulation with thermal feedback (where the time is 1.0 Gyr). On large scales, the velocity is broadly similar to the initial conditions. On smaller scales, however, there is an increase in the vertical velocity, which indicates the presence of an outflow, and the radial velocity, as material falls towards the black hole. The right-hand panel shows the corresponding vorticity profiles in cylindrical polar coordinates. The large-scale component is dominated by the rotation of the disc (and, as such, the z component of the vorticity) whilst on smaller scales, the effects of feedback create a more turbulent distribution, with a rising overall vorticity. The vertical dashed line indicates the edge of the refinement region. Our simulations without the refinement scheme (dashed lines) fail to capture much of this complexity.

simulations with thermal black hole feedback with super-Lagrangian refinement and without. This shows a problem with simulations without refinement – because the distribution is strongly peaked in the central region, the lack of resolution here leads to an underprediction of gas vorticity. We note here that this problem is just a manifestation of the different ways in which the simulations are capturing the gas properties around the black hole. Previous work (Curtis & Sijacki 2015, 2016) has shown that the increased resolution in the central region afforded by our refinement scheme can lead to significant differences in the capturing of the central feedback bubble and the subsequent transport of the feedback energy away from the immediate vicinity of the black hole.

More specifically, feedback has two effects: (a) it causes hot gas bubbles with low angular momentum to rise buoyantly away from the black hole on vertical (and partly radial) orbits and (b) it increases the sound speed of the gas, increasing turbulence that will drive viscous processes that may be responsible in part for transporting angular momentum outwards and mass inwards. This results in the gas in the central region having a very different velocity structure. For the cold, accreting gas, cells fall on to mostly radial orbits, implying $\omega_z \approx 0$, resulting in the drop in vorticity for the smallest radii. In addition, however, the strong black hole-driven outflow means that v_z has an R dependence in the innermost region. This results in a strong contribution to the vorticity from the azimuthal ω_ϕ term.

The left-hand panel of Fig. 6 shows the radial profiles of total gas vorticity for simulations with and without refinement at three different resolutions. The thick dot–dashed line is a simple analytic estimate of the vorticity profile which we calculate as follows: we assume that the dominant component in the vorticity signal is aligned with the z-axis of the disc and is dependent on the circular velocity, which we approximate as $\sqrt{GM(<R)/R}$. We then differentiate this field numerically to find the curl and, hence, the vorticity. All three refinement simulations at increasing resolutions produce very similar vorticity distribution and agree very well with our analytic estimate. Simulations without refinement, however, fail to reproduce inner vorticity peak a part from the highest resolution run. This indicates that for a comparable effective (large-scale) resolution and CPU resources, simulations without refinement are bound to systematically underestimate gas vorticity. This is illustrated explicitly in the right-hand panel of Fig. 6 where kernel averaged vorticity measurement is plotted as a function of simulated time. Not only is the estimated vorticity systematically smaller in the runs without refinement, but as we probe regions closer to the Bondi radius the estimate is dominated by the numerical noise (dashed blue line), demonstrating that much higher effective (and computationally more expensive) simulations would be needed to mitigate this issue.

5 SIMULATION RESULTS: IMPLICATIONS FOR BLACK HOLE GROWTH

5.1 Isolated disc galaxies

Fig. 7 shows the effects of our vorticity prescription on the evolution of the black hole mass in the isolated disc galaxy simulations. In the left-hand panel, we show the results for simulations with black hole feedback. Here, we can see that for standard isotropic thermal feedback, as expected from our analytic analysis, the suppression of the black hole growth is minimal. The surrounding gas is at too high a sound speed and as highlighted by Fig. 1 this simulation model probably represents the worst case for vorticity-based accretion suppression to be effective.

For comparison, we also show a simulation run using bipolar feedback, which has the effect of decoupling (to a certain extent) the black hole heated gas from the cold accreting gas. Here, we

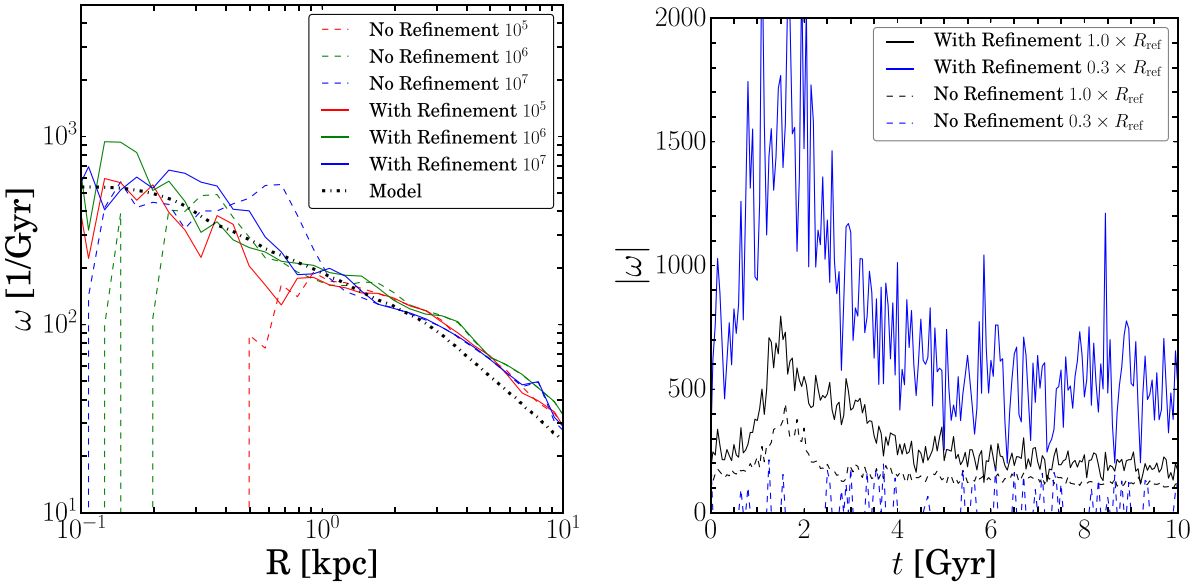

Figure 6. The left-hand panel shows radial profiles of total vorticity for simulations with (continuous lines) and without (dashed lines) refinement, both performed at three different resolutions. While all simulations have comparable vorticity profiles for $R > 1$ kpc, in the inner regions only the highest no refinement simulation produces vorticity profile which is comparable to all three resolution runs with refinement. The thick dot–dashed line shows a simple analytic vorticity profile which agrees with the results of our refinement simulations very well. The right-hand panel shows the time evolution of the kernel averaged vorticity measurement with refinement (continuous lines) and without (dashed). For both simulations two examples of estimates are shown: averaging over the full refinement region, i.e. a sphere with radius $R_{\rm ref}$ (black lines), and over a sphere with radius $0.3\,R_{\rm ref}$ (blue lines). The simulation with refinement not only captures a systematically higher vorticity across the whole simulated time-span, but it provides numerically meaningful results as we probe regions closer to the black hole's Bondi radius, while the simulation without refinement fails in this regime at the matching effective resolution.

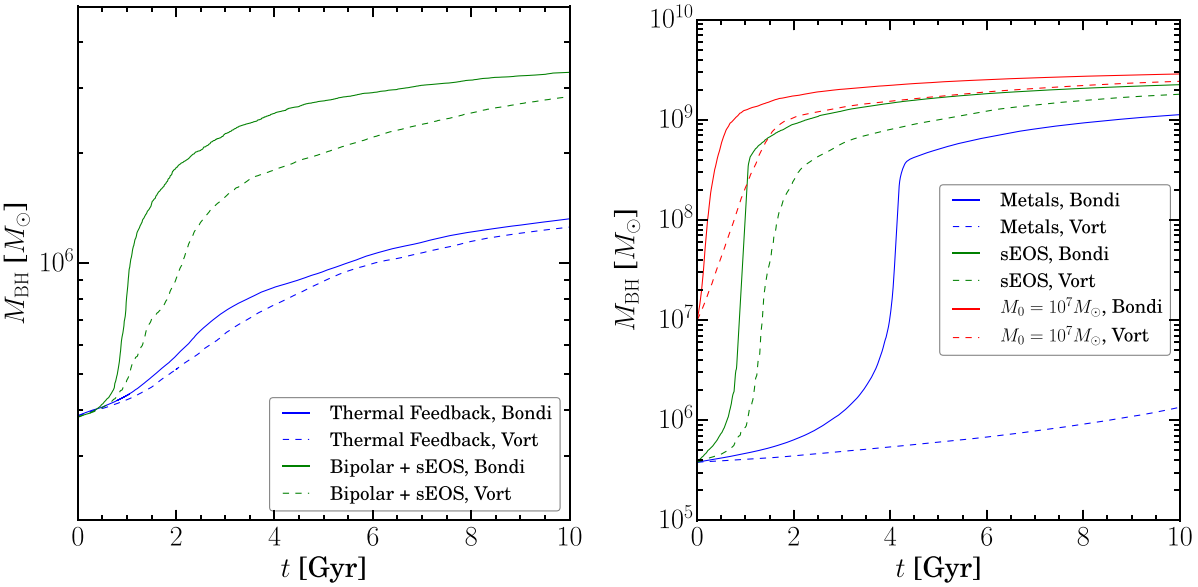

Figure 7. The left-hand panel shows the growth of black holes in simulations with two feedback prescriptions: thermal and bipolar coupled with a sEOS, taking into account the vorticity-based and standard Bondi accretion prescriptions. In the case of the thermal feedback, the sound speed is too high to allow for significant suppression by vorticity. In the bipolar case, whilst the black holes reach a similar final mass (which is determined in a large part by the cumulative energy injected by the feedback) there is a delay in the initial growth of the black hole of up to ∼1 Gyr. The right-hand panel shows the growth of black holes in simulations without feedback. In these cases, despite the black hole growth frequently being in the regime of significant suppression due to vorticity, the accretion rate is sufficiently high that the black holes grow quickly regardless. The exception to this is the simulation with metal line cooling, where all the relevant parameters remain in the critical region, as discussed in Section 3 (see Fig. 2).

adopt a softer equation of state for the ISM as well, leading to a less pressurized and more clumpy medium. The relative suppression of the black hole growth is more significant – indeed, at its peak $\dot{M}_{\rm Vort}$ is around one tenth of the standard Bondi rate – and has a noticeable effect especially at early times, with the peak growth phase of the black hole delayed by around 1 Gyr in the vorticity-based simulation. Note however that the final black hole masses are broadly independent of the accretion rate prescription (and much

more dependent on the feedback prescription) as black holes enter into self-regulated growth regime in both of these simulation models. Black hole growth is thus essentially determined by the amount of injected energy. In these cases, therefore, the suppressing effect of gas vorticity is sub-dominant compared to the feedback choice.

Given the strong dependence on feedback, we now turn to investigate the effect of the suppression in simulations with no feedback, in order to restrict our analysis to the effects of the accretion rate alone. Whilst such simulations have been shown to be unrealistic in many ways, they nevertheless provide insight into the different regimes of black hole growth in a simplified scenario. Specifically, while it is desirable on both theoretical and numerical grounds for the black hole growth to be self-regulated, in reality this is not necessarily the case, or it may occur on average with short, intermittent phases of rapid, unrestricted growth in between. Thus, our simulations without feedback and with strong self-regulation may each possibly book-end a more realistic scenario.

In the right-hand panel of Fig. 7, we show the evolution of the black hole mass for simulations without feedback, for three different setups: a fiducial simulation (which includes metal line cooling), a simulation with a softer equation of state and finally a simulation with a larger initial black hole mass of 10^7 $M_\odot$. Here, we are motivated by exploring different regimes that may lead to significant suppression, according to our previous analysis in Section 3. Black holes in simulations with a higher initial seed mass and with the softer equation of state grow rapidly, showing a very modest difference between the standard and vorticity simulations. This is despite the fact that in both cases, at its peak, the ratio of the vorticity-based prescription to the standard Bondi rate is around 0.01. The reason for this is that, in both cases, the fast black hole growth is driven by changes in the Bondi-part of the accretion rate (also due to a strong $M_{\rm BH}^2$ dependence) leading quickly to the Eddington-limited growth, to the extent that even a significant vorticity-based suppression has a limited effect on the overall evolution. For the simulation with metal line cooling, however, it is possible to enter a regime where the black hole growth is significantly suppressed by roughly three orders of magnitude and for the entire 10 Gyr of simulated timespan. While this highlights that gas angular momentum barrier can be extremely efficient in limiting black hole growth, we stress that the relevance of this result is clearly highly dependent on the actual gas properties on parsec scales and below, which are currently not well understood.

5.2 Merging galaxy pairs

In order to study the effects of our vorticity-based prescription on a situation where the angular momentum profile of the gas in the galaxy is significantly disrupted, we perform simulations of galaxy binary mergers. Here, we set up two galaxies with the same parameters as those in Section 2.3 at a distance of 200 kpc, which places them outside their respective virial radii. The two galaxies are initially in the same plane and collide on a prograde parabolic orbit. We limit ourselves here to studying the most interesting setup from our original simulations that gives a significant suppressing effect, namely one with no black hole feedback and with metal line cooling.

As the merging galaxies approach each other, they slow down due to dynamical friction and after two close passages they coalesce to form a spheroidal remnant.[2] Large-scale gravitational torques during the merging process funnel gas towards the innermost regions thus increasing the gas density around black holes as well as increasing the relative fraction of gas on radial versus azimuthal orbits. In the top row of Fig. 8, we show a selection of projected gas density maps from different stages of the merger evolution. The corresponding Voronoi tessellations of the computational domain are plotted in the second row. The first galaxy passage happens at around 0.5 Gyr, followed by a second passage at around 1.5 Gyr, leading to the binary black hole coalescence at around 2 Gyr.

During the merger a significant amount of gas is driven on to low angular momentum orbits, as illustrated in the third row of Fig. 8. Here, we plot the gas density measured within the black hole's smoothing length as a function of time. For comparison, we also show gas density from the isolated disc galaxy simulations using the same physics. The initial gas density evolution is identical, but at the first merger passage a large influx of gas increases the central density by around two orders of magnitude in the merger runs, which drives initial black hole growth in the standard Bondi simulation. Note that in the corresponding simulation with vorticity-based accretion rate prescription this initial black hole growth is suppressed, as gas has still a moderate vorticity. Large-scale torques during the second passage drive yet more gas towards the central region not long after the final merger of the two black holes, and this leads to a period of rapid, Eddington-sustained growth in the simulation with the standard Bondi rate. As black hole growth is not feedback regulated, central gas density quickly drops in the Eddington phase as the black hole is efficiently swallowing its surrounding gas reservoir.

This considerable angular momentum transport also has the effect of allowing the black hole with the vorticity-based accretion rate prescription to grow to a significantly higher mass than in the isolated disc galaxy case, as the central gas density stays about an order of magnitude higher. However, the black hole growth is modulated by the presence of non-zero gas vorticity. This leads to a delay of more than 2 Gyr before the Eddington-limited phase is reached, which ultimately leads to the final black hole mass similar to, albeit somewhat smaller than, the standard Bondi case. This effect is very interesting as it leads to a large time-offset between the peak in star formation activity (which occurs at 0.7 Gyr) and the peak in black hole growth and thus the occurrence of the quasar phase. Taken at the face value, this could also explain the observational lack of evidence that the quasar triggering occurs in host galaxies with perturbed morphologies: in the vorticity-based prescription major black hole growth occurs at around 5.5 Gyr when the galaxy merger remnant is largely relaxed and spherical (see right-hand top panel of Fig. 8).

Whilst during the merger large-scale torques clearly channel much of the gas on to low angular momentum orbits, allowing it to move to within the accreting region of the black hole, we find that the effects of this are not significant enough to completely overcome the suppression encoded in our vorticity-based prescription, i.e. that the inner gas flow is not purely radial. This is, perhaps, unsurprising since the condition in 2.2.1.1 is especially stringent. Although to a certain extent, we are limited by our finite resolution and numerical precision given the relatively tiny size of the Schwarzschild radius, more generally it is worth stressing that the validity of our results is restricted by poorly known gas properties on spatial scales of

[2] Note that due to the relative orientation of galaxies in this specific merger setup, a gaseous disc reforms during the intermediate stage of the merger, which has considerable vorticity.

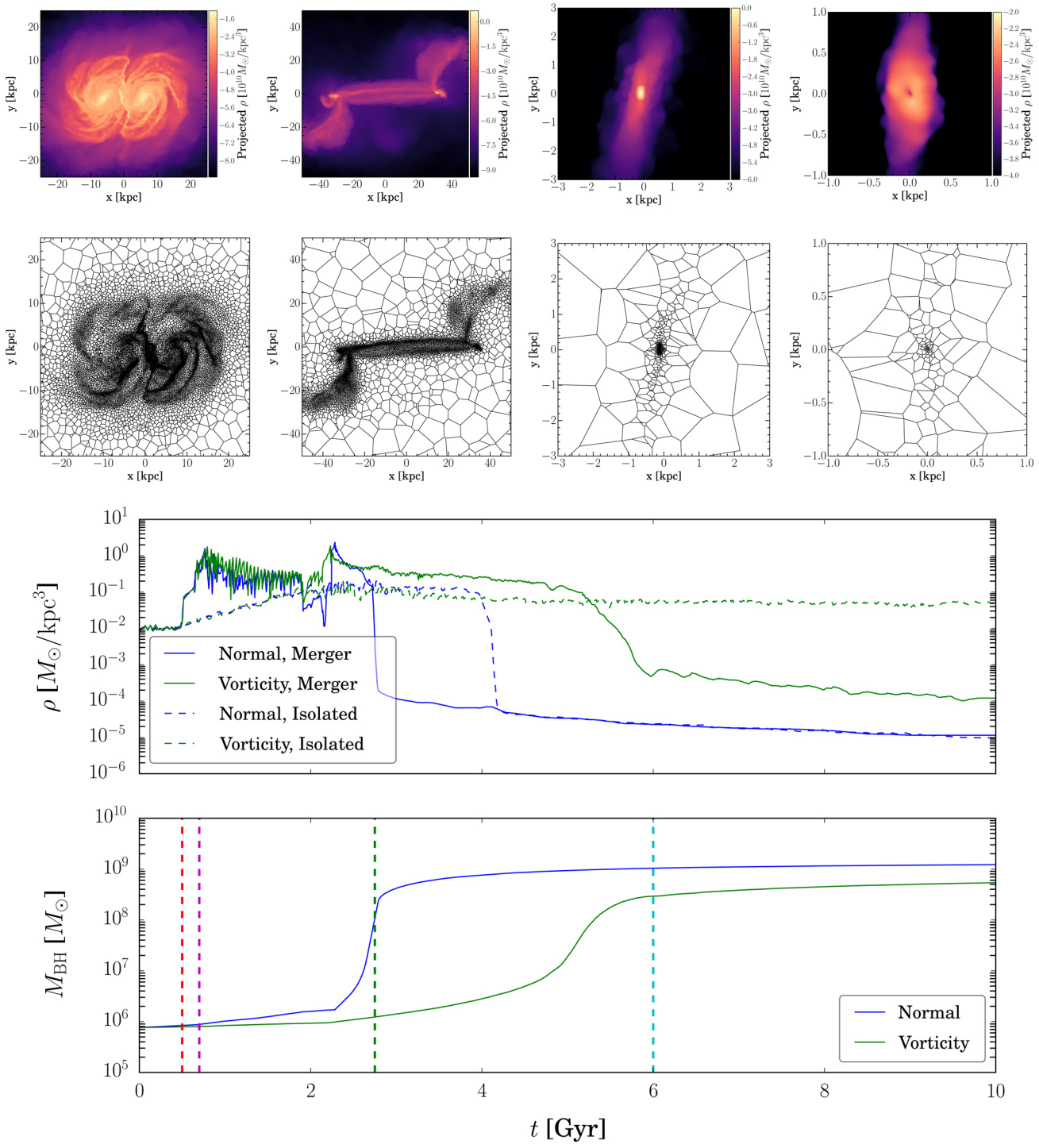

Figure 8. The top row shows the projected gas density of our simulations of a galaxy merger pair at times of 0.5, 0.7, 2.75 and 6 Gyr (from left to right), spanning a time sequence from the first contact to the final merger remnant. The second row shows the corresponding Voronoi mesh, which illustrates the spatial resolution of our hydro solver. Below this, the evolution of the gas density within the black hole's smoothing length is plotted, including the case with the standard Bondi accretion prescription (blue) and with the vorticity-based prescription (green). For comparison, we plot the same quantity from our simulations of isolated disc galaxies simulated with the same physics (dashed lines). Finally, the bottom row shows the evolution of the black hole mass for our merger simulations with Bondi and vorticity-based prescriptions (dashed vertical lines correspond to the image sequence shown in the top row). While there is a significant delay in black hole growth after the second passage with vorticity-based prescription, due to the large-scale torques high gas central density builds up, which ultimately leads to the final black hole mass similar as in the standard Bondi case.

parsecs and below, where gas fragmentation, star formation and their associated feedback, as well as the nature of the gas flow on even smaller scales (e.g. in the 'alpha-disc' regime) may dominate the final supply rate to the black hole.

6 CONCLUSIONS

In this paper we have investigated the impact of gas angular momentum on the growth of supermassive black holes. Specifically, we have limited our analysis to the model initially proposed by Krumholz et al. (2005) that takes into account gas vorticity as to generalize the well-known Bondi accretion rate. While by no means exhaustive, this model is well suited for implementation in galaxy formation simulations, especially in the case where the relevant gas properties are robustly measured close to the Bondi radius, which is the case when we adopt our super-Lagrangian refinement technique (Curtis & Sijacki 2015). Note that the refinement is not only needed to accurately measure gas density and sound speed, but the gas vorticity field itself, which is even more numerically challenging. We have implemented this vorticity-based accretion rate prescription in the moving mesh code AREPO, for general usage in (cosmological) galaxy formation simulations. We have extensively tested our implementation on a range of numerically challenging setups obtaining robust results and have verified the convergence properties of the model with increasing resolution.

With respect to the Bondi rate, in the vorticity-based prescription a significant suppression of black hole growth is expected when gas angular momentum and thus vorticity are high. To fully investigate model predictions we have first developed simple analytical dynamical models, which allowed us to establish a tight dependence of the relative suppression magnitude on the density and sound speed of the gas – two properties that on the scales of interest are poorly constrained in practice by both observations and simulations. Moreover, due to the significant dependence of the accretion rate on the black hole mass ($\propto M_{\rm BH}^2$), our dynamical models reveal a more nuanced effect, whereby significant accretion suppression can be outweighed by rapid growth in cases where the net accretion rate is high (i.e. close to the Eddington limit).

We have then explored the effects that different black hole feedback parametrizations and ISM physics choices have on the black hole growth with the matching set of simulations of isolated disc galaxies, performed with the standard Bondi and vorticity-based accretion rate prescriptions. In doing so, we have found a picture that is broadly similar to our analytic predictions: black hole growth is largely governed by feedback but that, within this, the effect of the vorticity prescription is to have a mild suppression on the accretion rate. One of the principal reasons for this is the self-regulating nature of feedback implementations we considered in this study, where the final black hole mass is largely set by the amount of feedback energy injected.

Conversely, in simulations without black hole feedback, we found that the black hole can be in regimes where the suppressing effect is much more significant, even leading to no appreciable growth over a Hubble time. The contrasting no feedback and feedback simulation results are likely to bracket a more realistic scenario, where black hole self-regulation is not as tight as we assumed here and occurs on a natural duty cycle after longer episodes of sustained growth, when significant amounts of gas can be expelled in a large-scale outflow from the innermost region of the host galaxy.

Finally, we have studied the case of isolated binary major mergers of two disc galaxies hosting black holes. Due to very efficient torquing gas angular momentum is efficiently transported outwards and large amounts of gas are funnelled towards the centre of the merger remnant. With respect to the isolated disc galaxy model, the growth of the black hole using the vorticity prescription is greatly increased as expected, but it still remains significantly suppressed when compared to merger remnant grown with the standard Bondi rate. Interestingly, while the final black hole mass in the merger runs with and without vorticity suppression is similar, there is a several Gyr delay in reaching this mass, once the gas angular momentum barrier is taken into account. This could naturally explain scarce observational evidence of quasar triggering in galaxies with perturbed morphologies which previously had been accounted for by obscuration effects alone. Indeed, there is observational evidence of a significant delay between starburst activity and the peak of AGN activity (e.g. Davies et al. 2007; Bennert et al. 2008; Yesuf et al. 2014; Matsuoka et al. 2015).

We finally caution that our work is just a first stab in the direction of understanding the interplay between the black hole growth and the gas angular momentum from the point of view of galaxy formation simulations. As we have demonstrated in this work, the black hole accretion suppression within our model is highly sensitive on the gas properties on parsec scales. Thus a more realistic treatment of the ISM physics and black hole feedback are needed to make more progress on this front. More generally, the amount of gas that may eventually reach the black hole will be heavily modulated by the physics occurring on even smaller spatial spaces, where effectiveness of gas fragmentation, star formation (and stellar winds) as well as (magneto-) hydrodynamical viscous transport processes through the accretion disc need to be considered. While numerically self-consistently accounting for all these processes on such a vast range of spatial scales will be a formidable challenge for some time to come, simulations have now started to reach the regime where some of these scales can be bridged, promising to shed light on the physics that powers supermassive black hole growth.

ACKNOWLEDGEMENTS

We thank Ewald Puchwein, Martin Haehnelt and Volker Springel for their useful comments on our manuscript. We thank Ruediger Pakmor for proving us with his initial condition setup for the Keplerian disc simulation. MC is supported by the Science and Technology Facilities Council (STFC). DS acknowledges support by the STFC and the ERC Starting Grant 638707 'Black holes and their host galaxies: co-evolution across cosmic time'. This work was performed on the following: the COSMOS Shared Memory system at DAMTP, University of Cambridge operated on behalf of the STFC DiRAC HPC Facility – this equipment is funded by BIS National E-infrastructure capital grant ST/J005673/1 and STFC grants ST/H008586/1, ST/K00333X/1; DiRAC Darwin Supercomputer hosted by the University of Cambridge High Performance Computing Service (http://www.hpc.cam.ac.uk/), provided by Dell Inc. using Strategic Research Infrastructure Funding from the Higher Education Funding Council for England and funding from the Science and Technology Facilities Council; DiRAC Complexity system, operated by the University of Leicester IT Services. This equipment is funded by BIS National E-Infrastructure capital grant ST/K000373/1 and STFC DiRAC Operations grant ST/K0003259/1; COSMA Data Centric system at Durham University, operated by the Institute for Computational Cosmology on behalf of the STFC DiRAC HPC Facility. This equipment was funded by a BIS National E-infrastructure capital grant ST/K00042X/1, STFC capital grant ST/K00087X/1, DiRAC

Operations grant ST/K003267/1 and Durham University. DiRAC is part of the National E-Infrastructure.

REFERENCES

Abramowicz M. A., Zurek W. H., 1981, ApJ, 246, 314
Abramowicz M. A., Chen X., Kato S., Lasota J.-P., Regev O., 1995, ApJ, 438, L37
Balbus S. A., Hawley J. F., 1991, ApJ, 376, 214
Barnes J. E., Hernquist L. E., 1991, ApJ, 370, L65
Bennert N., Canalizo G., Jungwiert B., Stockton A., Schweizer F., Peng C. Y., Lacy M., 2008, ApJ, 677, 846
Birnboim Y., Dekel A., 2003, MNRAS, 345, 349
Blandford R. D., Begelman M. C., 1999, MNRAS, 303, L1
Bondi H., 1952, MNRAS, 112, 195
Bondi H., Hoyle F., 1944, MNRAS, 104, 273
Cullen L., Dehnen W., 2010, MNRAS, 408, 669
Curtis M., Sijacki D., 2015, MNRAS, 454, 3445
Curtis M., Sijacki D., 2016, MNRAS, 457, L34
Davies R. I., Müller Sánchez F., Genzel R., Tacconi L. J., Hicks E. K. S., Friedrich S., Sternberg A., 2007, ApJ, 671, 1388
Di Matteo T., Springel V., Hernquist L., 2005, Nature, 433, 604
Dubois Y., Pichon C., Devriendt J., Silk J., Haehnelt M., Kimm T., Slyz A., 2013, MNRAS, 428, 2885
Emsellem E., Renaud F., Bournaud F., Elmegreen B., Combes F., Gabor J. M., 2015, MNRAS, 446, 2468
Frank J., King A., Raine D. J., 2002, Accretion Power in Astrophysics, 3rd edn. Cambridge Univ. Press, Cambridge
Goodman J., 2003, MNRAS, 339, 937
Hernquist L., 1989, Nature, 340, 687
Hernquist L., 1990, ApJ, 356, 359
Hobbs A., Nayakshin S., Power C., King A., 2011, MNRAS, 413, 2633
Hopkins P. F., 2015, MNRAS, 450, 53
Hopkins P. F., Quataert E., 2010, MNRAS, 407, 1529
Hoyle F., Lyttleton R. A., 1939, Proc. Camb. Phil. Soc., 34, 405
Kereš D., Katz N., Weinberg D. H., Davé R., 2005, MNRAS, 363, 2
Kewley L. J., Groves B., Kauffmann G., Heckman T., 2006, MNRAS, 372, 961
King A. R., Pringle J. E., 2006, MNRAS, 373, L90
Knapen J. H., Shlosman I., Peletier R. F., 2000, ApJ, 529, 93
Krumholz M. R., McKee C. F., Klein R. I., 2005, ApJ, 618, 757
Krumholz M. R., McKee C. F., Klein R. I., 2006, ApJ, 638, 369
Laine S., Shlosman I., Knapen J. H., Peletier R. F., 2002, ApJ, 567, 97
Levine R., Gnedin N. Y., Hamilton A. J. S., Kravtsov A. V., 2008, ApJ, 678, 154
Lo K. Y., 2005, ARA&A, 43, 625
Matsuoka Y. et al., 2015, ApJ, 811, 91
Mayer L., Kazantzidis S., Madau P., Colpi M., Quinn T., Wadsley J., 2007, Science, 316, 1874
Monaghan J. J., Lattanzio J. C., 1985, A&A, 149, 135
Narayan R., Yi I., 1995, ApJ, 452, 710
Nelson D., Genel S., Vogelsberger M., Springel V., Sijacki D., Torrey P., Hernquist L., 2015, MNRAS, 448, 59
Pakmor R., Springel V., Bauer A., Mocz P., Munoz D. J., Ohlmann S. T., Schaal K., Zhu C., 2016, MNRAS, 455, 1134
Power C., Nayakshin S., King A., 2011, MNRAS, 412, 269
Pringle J. E., 1981, ARA&A, 19, 137
Proga D., Begelman M. C., 2003, ApJ, 582, 69
Roberts W. W., Jr, Huntley J. M., van Albada G. D., 1979, ApJ, 233, 67
Rosas-Guevara Y. M. et al., 2015, MNRAS, 454, 1038
Russell H. R., Fabian A. C., McNamara B. R., Broderick A. E., 2015, MNRAS, 451, 588
Shakura N. I., Sunyaev R. A., 1973, A&A, 24, 337
Shlosman I., Frank J., Begelman M. C., 1989, Nature, 338, 45
Sijacki D., Springel V., Di Matteo T., Hernquist L., 2007, MNRAS, 380, 877
Springel V., 2010, MNRAS, 401, 791
Springel V., Hernquist L., 2003, MNRAS, 339, 289
Springel V., Di Matteo T., Hernquist L., 2005, MNRAS, 361, 776
Thompson T. A., Quataert E., Murray N., 2005, ApJ, 630, 167
van de Voort F., Schaye J., Booth C. M., Haas M. R., Dalla Vecchia C., 2011, MNRAS, 414, 2458
Vogelsberger M., Genel S., Sijacki D., Torrey P., Springel V., Hernquist L., 2013, MNRAS, 436, 3031
Xu Y.-D., Narayan R., Quataert E., Yuan F., Baganoff F. K., 2006, ApJ, 640, 319
Yesuf H. M., Faber S. M., Trump J. R., Koo D. C., Fang J. J., Liu F. S., Wild V., Hayward C. C., 2014, ApJ, 792, 84
Yuan F., Quataert E., Narayan R., 2003, ApJ, 598, 301

APPENDIX A: SETTING THE $f_{\rm sort}$ THRESHOLD

As discussed in Section 4.2, $f_{\rm sort}$ is the fraction of the gas mass that has a vorticity within $\pi/4$ of the direction of the net vorticity. We set a minimum value that represents the threshold for using our vorticity prescription.

Fig. A1 shows the distribution of the fraction of gas which is aligned with the net vorticity for simulations of Bondi flow, as well as for simulations of isolated disc galaxies with and without feedback. In the case of the Bondi simulation, the vorticity signal is noise driven and so the fraction aligned with the net vorticity follows that expected for a random distribution. In the case of the disc galaxy, the signal is coherent, especially when there are no perturbations to the velocity field caused by feedback. We set the threshold at which the vorticity suppression is active to be $f_{\rm sort} = 0.35$, to exclude the scenario present in the Bondi simulations.

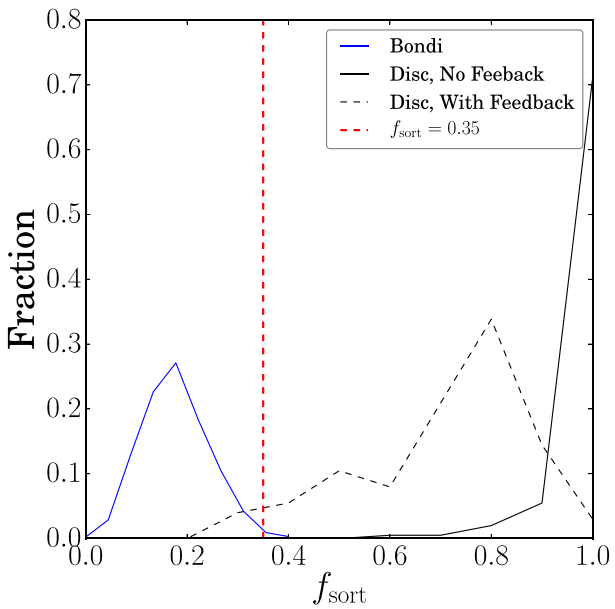

Figure A1. The distribution of $f_{\rm sort}$ for simulations of Bondi flow, as well as simulations of isolated disc galaxies with and without feedback.

This paper has been typeset from a TEX/LATEX file prepared by the author.